Seismic ground roll absorption and re-emission by sand dunes

M. I. Arran[1,2], N. M. Vriend[1], E. Muyzert[2]

[1]Department of Applied Maths and Theoretical Physics, University of Cambridge, Cambridge, UK
[2]Schlumberger Cambridge Research, Cambridge, UK

Key Points:

- In seismic surveys, sand dunes will exhibit absorption and reemission of ground-roll, causing noise.
- We present a simple analytic model that successfully predicts the amplitude of this noise.
- The noise is lower upwind of a barchan dune, and away from a resonant frequency of the dune.

Corresponding author: M. I. Arran, `mia31@damtp.cam.ac.uk`

Abstract

Ground roll is a significant source of noise in land seismic data, with crossline scattered ground roll particularly difficult to suppress. This noise arises from surface heterogeneities lateral to the receiver spread, and in desert regions sand dunes are a major contributor. However, the nature of this noise is poorly understood, preventing the design of more effective data acquisition or processing techniques. Here, we present numerical simulations demonstrating that a barchan sand dune acts as a resonator, absorbing energy from ground roll and reemitting it over an extensive period of time. We derive and validate a mathematical framework that quantitatively describes the properties of the emitted waves, and demonstrate that wave amplitude is estimable from easily-measurable bulk properties of the dune. Having identified regions in time, space, and frequency space at which noise will be more significant, we propose reducing dune-scattered noise through careful survey design and data processing. In particular, we predict that seismic noise will be lower upwind of barchan dunes, and at frequencies far from a 'resonant' frequency $2c_S/H$, for dune height H and typical seismic velocity within the dune c_S. This work is especially relevant to seismic acquisition in the vicinity of a dune field, where scattered noise appears incoherent and difficulties arise with alternative approaches to noise suppression.

1 Introduction

Sand dunes cause noise in seismic surveys by scattering surficial Rayleigh waves. When surface sources are used in the acquisition of land seismic data, as in vibroseis and weight-drop surveys, approximately 2/3 of the energy delivered by the source propagates along the Earth's surface in the form of such waves [*Miller and Pursey*, 1955; *Richart et al.*, 1970], which are reflected or refracted where topography or seismic velocity at the surface varies [*Hudson and Knopoff*, 1967; *Levander*, 1990]. Since desert sand dunes are associated with topographical variation of tens or hundreds of meters and with considerably lower seismic velocities than surrounding bedrock [*Almalki and Alkhalifah*, 2012; *Zhou*, 2014], these dunes will reflect seismic signals on arrival, and absorb seismic energy that is subsequently re-emitted over time [*Combee*, 1994; *Ling et al.*, 1998; *Drummond et al.*, 2003]. This scattered energy will propagate to the seismic receiver spread as seismic noise, with again the preponderance of energy transmitted by surface waves. For distance traveled r, the amplitude of surface waves decays as $r^{-1/2}$ while the signal of interest is carried by body waves with amplitude decaying as r^{-1}, so the amplitude of this noise can be significantly higher than that of the signal, seriously degrading the quality of seismic data.

Established approaches often struggle to suppress this noise. Common workflows in hydrocarbon exploration include high-pass filters for frequency or apparent velocity, or multidimensional filters in f-k or τ-p space [*Chen et al.*, 2015; *Embree et al.*, 1963; *Kirchheimer*, 1985; *Hu et al.*, 2016; *Xu et al.*, 2016]. However, there is significant overlap between the frequency range of industry-relevant signals and that of ground roll. Furthermore, a dune lateral to the principle direction of a receiver spread will scatter ground roll crossline, resulting in a high apparent velocity and hence poor noise suppression. 3D surveys permit removal of ground roll with a general direction of incidence [*Vermeer*, 2012; *Regone*, 1997], but adequate suppression requires large receiver arrays, increasing financial costs, decreasing spatial resolution, and attenuating high-frequency components of the signal [*Cordsen and Galbraith*, 2002].

More recent approaches include interferometric ground-roll removal [*Dong et al.*, 2006; *Halliday et al.*, 2010, 2015] and polarization filtering [*Flinn*, 1965; *Kragh and Peardon*, 1995; *Tiapkina et al.*, 2012], but these are also imperfect solutions. Successful interferometric noise suppression relies on an acquisition geometry adapted to the positions of scatterers, so that scattered surface waves pass through a 'boundary' of receivers before arriving at the receiver at which noise is to be suppressed [*Forghani and Snieder*, 2010]. Polarization filtering, meanwhile, imposes the additional expenses associated with three-component receivers and loses effectiveness in the case of simultaneous arrivals [*Jackson et al.*, 1991; *Tiapkina et al.*, 2012]. Both will, therefore, struggle to adequately suppress noise in the case of a complex geometry of multiple scatterers, such as a desert dune field.

With generic approaches to ground-roll suppression having difficulties in the case of scattering by dunes, the modeling of the scattering process has fundamental importance. Dune-scattered ground roll will contribute differently to recorded displacements in different regions of time, space, and frequency-wavenumber space, and such modeling will allow these different contributions to be quantified. This quantification is key to the design of surveys and to the interpretation of data. However, to successfully model scattering from dunes, we must first describe their attributes.

We focus on isolated crescentic barchan dunes, which are both sufficiently simple in form to be amenable to analysis, and sufficiently common for such analysis to have application in regions of potential hydrocarbon exploration. Sand dunes in deserts arise from the transport of sediment by the wind, and in different regimes of sediment supply and wind variability, a variety of dune morphologies can exist [*Bagnold*, 1941; *Holm*, 1960; *McKee*, 1979, 1982], but in many such regions the wind is approximately unidirectional, sand supply is limited, and barchan dunes predominate. Specific examples include Kuwait's major Al-Huwaimiliyah dune field [*Al-Dabi et al.*, 1997], the Najaf and Nasiriyah dune fields of Iraq [*Jawad Ali and Al-Ani*, 1983], both the Eastern and Western dune fields of Qatar [*Ashour*, 1987], and the northern portion of the UAE's Al Liwa basin [*Bishop*, 2013]. Barchan dunes are characterized by a crescent-shaped brinkline, with height reaching a maximum at the crescent's center and decreasing towards the downwind-facing horns either side. On the windward side, sand is transported by the wind up a shallow slope of approximately 10°, while, on the leeward side, grains avalanche down a steep slip face at the sand's angle of repose, approximately 30°. Between dunes lies the exposed desert floor. An example is shown in Figures 1a and 1b. Dune length, width, and height are in approximately constant proportion, with heights from 1 m to over 100 m [*Finkel*, 1959; *Lancaster*, 1982; *El-Sayed*, 2000]. With barchans displaying less variation in shape than is typical of other types of dune, a smaller parameter space need be explored for applicability, while dunes' separation by the flat, exposed desert floor permits consideration of each dune in isolation.

Dunes are associated not only with topographical variation, but also with varation in seismic velocities. In the field, *Criswell et al.* [1975] measure a surface wave speed of 120 m s^{-1} on an aeolian desert dune, while, more recently, *Vriend et al.* [2015] measure a P wave speed of 200 ± 20 m s^{-1} in a near-surface layer and 350 ± 30 m s^{-1} in the bulk, with corresponding S wave speeds of 130 ± 20 m s^{-1} and 180 ± 20 m s^{-1}. Seismic velocities within the desert floor vary significantly depending on pressure and geological composition, but are typically much higher [*Bourbié et al.*, 1987], with the speed of S waves approximately three-fifths of that of P waves, based on a Poisson's ratio of 0.2 [*Gercek*, 2007].

In addition to varying between the dune and the desert floor, seismic velocities vary significantly within a dune. *Vriend et al.* [2007] observed variation of P wave speeds by a factor of around three, and explain this by variation in pressure and in water satura-

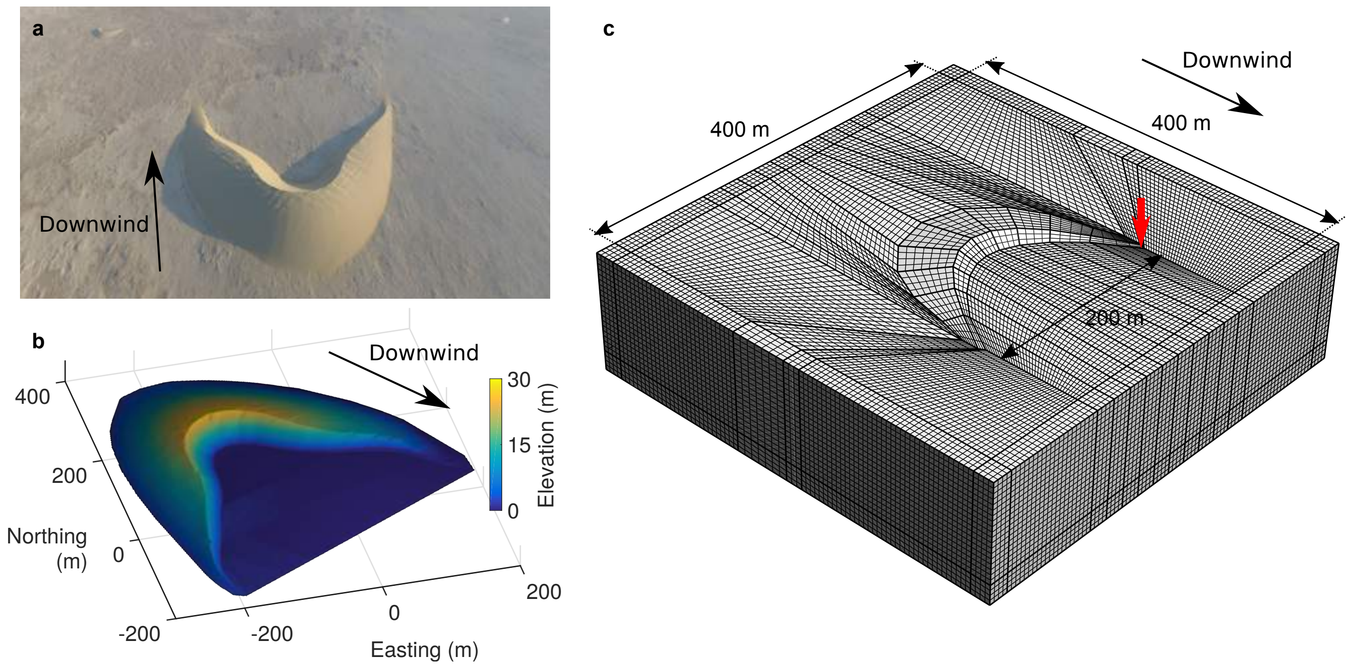

Figure 1. Barchan dune geometry, in reality (**a**, **b**) and our simulations (**c**). **a)** Image of an isolated Qatari barchan dune from an aerial drone, courtesy of Sylvain Michel. At top left and top right are neighboring dunes. **b)** Elevation profile of the same barchan, from data courtesy of Michel Louge. **c)** Mesh generated with GMsh, as described in section 2.1. The red arrow indicates the location of the point force for the simulations described in section 2.2 and depicted both in Figure 2 and in the movies in the supplementary materials.

tion. In the unconsolidated sand that forms desert dunes, seismic velocities increase with effective pressure p, and hence with depth in the dune. Variants of Hertz-Mindlin theory, assuming spherical particles and a constant contact network, predict seismic velocities to increase as $p^{1/6}$ [*Duffy and Mindlin*, 1956; *Walton*, 1987; *Mavko et al.*, 2003], while laboratory experiments instead find dependence of approximately $p^{0.25}$ or $p^{0.33}$ for S waves and $p^{0.23}$ or $p^{0.30}$ for P waves [*Hardin and Black*, 1968; *Yu and Richart*, 1984; *Zimmer et al.*, 2007; *Bodet et al.*, 2014]. While pressure in a granular medium is not necessarily equal to the weight of the overburden, as demonstrated by Janssen pressure saturation in silos [*Janssen*, 1895] and by the central pressure dip in sandpiles [*Smid and Novosad*, 1981], it is standard in geophysics to assume, in a medium of constant bulk density, direct proportionality between pressure and depth.

The distribution of water saturation within a dune cannot be so easily approximated, as it depends on historical rainfall and structure formation within the dune. *Berndtsson et al.* [1996] reported spatial varation of water content from 0.7% to 7.3% by volume, in a study area 3 m deep and 60 m wide on an unvegetated dune in Northwestern China, with rainfall preferentially permeating pre-existing layers. On a smaller scale, in 0.45 m by 2.5 m vertical sections on five dunes in southwestern North America, *Ritsema and Dekker* [1994] reported variation from 2.0% to 12.6%, 2% to 8.3%, 0.6% to 11.1%, 0.6% to 11.1% and 0.6% to 5.3%, with wetter regions irregularly positioned at greater depth, representing "a residual stage from former rain events". Studies report similar orders of magnitude of variation in desert dunes in Saudi Arabia [*Dincer et al.*, 1974] and Algeria [*Fontes et al.*, 1986], and variation an order of magnitude smaller in Qatar [*Louge et al.*, 2013]. That this variation coincides with dunes' internal structure is confirmed by studies with ground-penetrating radar, in which variation of moisture content is associated with strong reflections, revealing the cross-bedding laid down within the dune [*Schenk et al.*, 2009; *Bristow et al.*, 1996; *Qian et al.*, 2014; *Neal*, 2004]. This cross-bedding will, therefore, be associated with variation in seismic velocity.

We structure this paper in the following manner. Section 2 describes the development of a model for the scattering of surface waves by a solitary barchan dune, with an initial investigation, described in section 2.2, inspiring the development of an analytical model, in section 2.3. In section 3, we validate the model, confirming its assumptions and ascertaining the values of its parameters in section 3.1; and testing its predictions of the noise observed at receivers in section 3.2. In section 4, we examine the effect of varying the parameters of our system: dune geometry in section 4.1 and internal structure in section 4.2. Finally, in section 5, conclusions are drawn, future work discussed, and industry-relevant outputs assessed.

2 Model development

2.1 Numerical modelling

To examine the effect of a barchan dune on seismic propagation, we conduct numerical simulations using SPECFEM3D, a parallelized open-source software package which uses the continuous Galerkin spectral-element method, with Gauss-Lobatto-Legendre quadrature [*Tromp et al.*, 2008; *Komatitsch et al.*, 2002; *Peter et al.*, 2011]. We use spectral elements of degree 5, neglect attenuation and anisotropy, and simulate absorbing boundaries with convolutional perfectly matched layers (CPML) [*Komatitsch and Martin*, 2007]. GMsh, a three-dimensional finite-element mesh generator [*Geuzaine and Remacle*, 2009], is used to create structured hexahedral meshes for the desired geometry. A mesh refinement study is described in Appendix A, demonstrating that a typical mesh spacing of half the dune height is sufficient for 10% accuracy in displacement.

We construct meshes such as that shown in Figure 1c, with a crescentic brinkline achieving a maximum height H at its center. All meshes are 400 m long, 400 m wide, and 100 m deep, with a typical mesh spacing of 5 m and CPML 4 grid points thick on each side, sufficient for over 99% of the energy reaching the mesh's boundaries to be absorbed (calculated as described in Appendix B). The brinkline has coordinates $(X(\cosh(\alpha y/Y)-1)/(\cosh(\alpha)-1), y, H\cos(\pi y/2Y))$ in the range $|y| < Y$, for constants X, Y, H, and $\alpha = 1/2$, so that the horns are advanced a distance X downwind of the crest and have a separation of $2Y$. Tangential to the brinkline, angles of inclination on the windward and leeward faces are 10^o and 30^o respectively. This geometry reproduces the features of barchan dunes, while permitting the construction of structured meshes that satisfy the conditions of SPECFEM3D and are sufficiently regular for simulations to converge.

Throughout this work, we use point sources located at a depth of 1 m, to mimic the surface sources used in contemporary seismic surveys, while avoiding the numerical instability associated with simulating a source at the mesh boundary.

2.2 Initial simulation

To identify the processes that underlie the scattering of ground-roll by dunes, we conduct an initial simulation. We construct the mesh shown in Figure 1c, with geometry as defined in section 2.1 and parameters $H = 10$ m, $X = 100$ m, and $Y = 100$ m. We model both the dune and the desert floor as isotropic and homogeneous media. Within the desert floor, we model P and S wave velocities as 1000 and 600 m s^{-1}, respectively, whilst within the dune we model P and S wave velocities as $c_P = 350$ and $c_S = 180$ m s^{-1}, respectively. For simplicity, density is everywhere 2500 kg m^{-3}. We simulate a vertical point force of amplitude 10^3 N, 100 m downwind of the dune's crest and 100 m off its central axis, with time-dependency given by a Ricker function wavelet with central frequency 10 Hz. A movie showing vertical displacement at the surface is shown in the supplementary materials, with selected frames reproduced below in Figure 2, Panel a. For comparison, we also conduct simulations of a model with identical topography, but with seismic velocities in the dune equal to those in the desert floor (Panel b); and of a homogeneous halfspace of equal size (Panel c).

We observe significant scattering by the sand dune over an extended period of time, with the majority of this scattering related to the difference in seismic velocities between the sand dune and the desert floor. Considering individual wave packets over time, we see that those reaching the dune are either reflected from or transmitted through its boundary. Transmitted energy propagates within the dune, with a certain proportion emitted each time the boundary is reached. The complex geometry of the dune causes that proportion of the wave packet that is retained within the dune to lose coherence over time, resulting in a distribution of energy only weakly corresponding to initial conditions, decaying primarily through emission of surface waves.

2.3 Analytical model

Given the observations described above, we propose a highly simplified model for seismic propagation in the vicinity of a dune, illustrated schematically in Figure 3. We suppose that a source at position $\mathbf{x}_S$ emits surface waves of frequency f in some short time window about t_S, with total energy E_S emitted as Rayleigh waves.

Assuming isotropic radiation and no attenuation over a homogeneous desert floor with Rayleigh wave speed c_R, the energy reaching a dune subtending angle Φ_D, of lat-

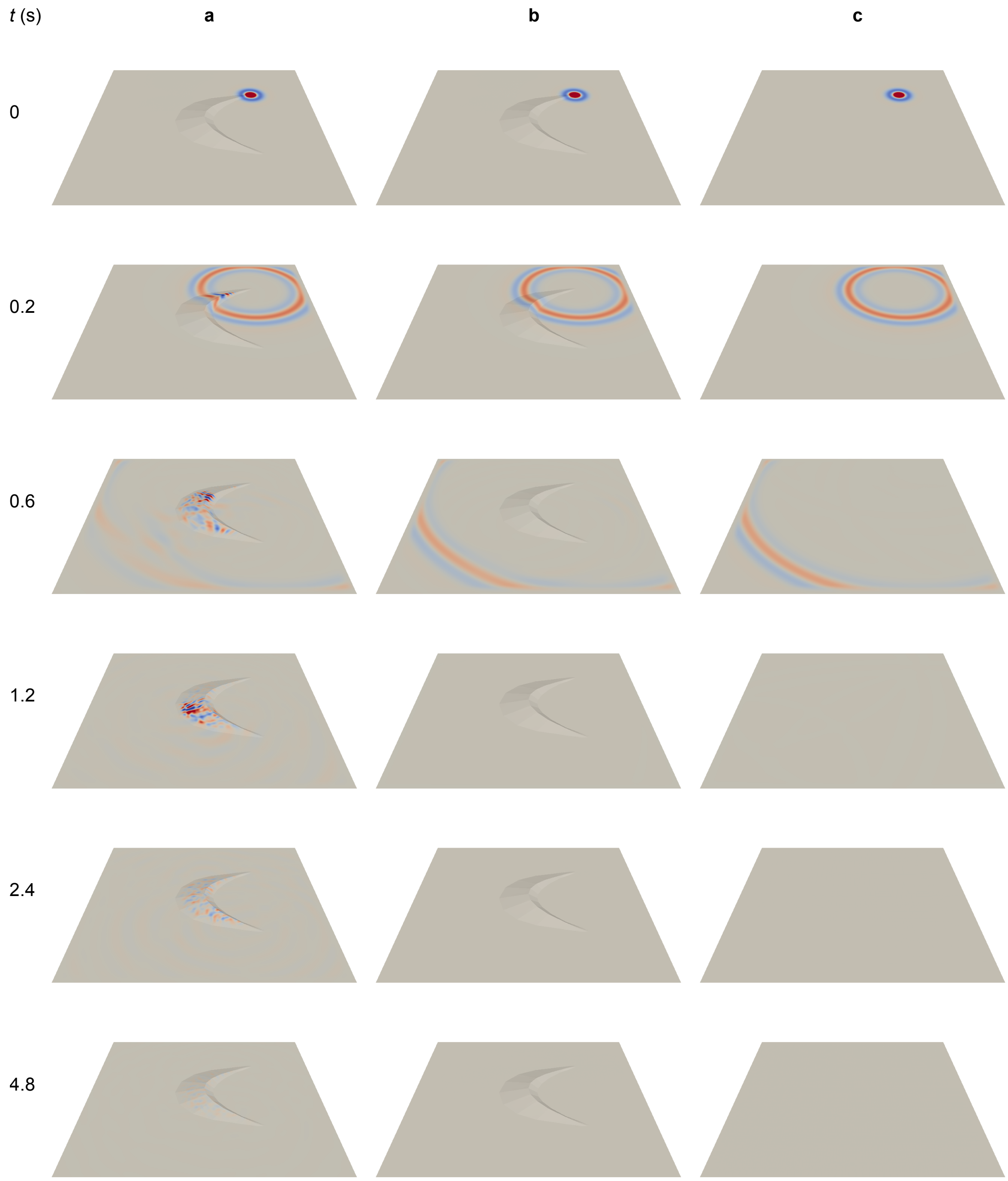

193 **Figure 2.** Color maps of vertical displacement on the surface of a homogeneous halfspace,
194 surmounted by **a)** a dune with distinct seismic velocities, **b**) a dune having equal seismic veloci-
195 ties, and **c**) nothing. The halfspace has P and S wave velocities 1000 and 600 m s^{-1} respectively,
196 while in **a** the dune has P and S wave velocities of 350 and 180 m s^{-1} respectively.

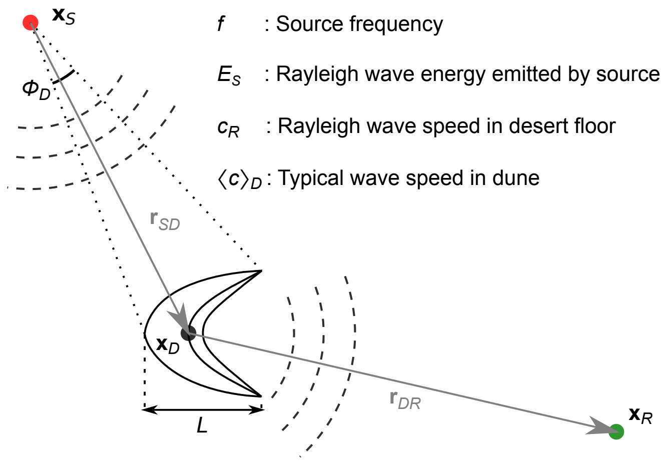

Figure 3. Schematic of wave scattering by a dune, with definitions of relevant variables.

eral extent L and with crest position $\mathbf{x}_D = \mathbf{x}_S + \mathbf{r}_{SD}$, will be

$$\frac{E_S \Phi_D}{2\pi} \approx \frac{E_S L}{2\pi ||\mathbf{r}_{SD}||}. \tag{1}$$

The arrival time will be approximately $t_S + ||\mathbf{r}_{SD}||/c_R$, with approximations exact in the far-field limit $||\mathbf{r}_{SD}||/L \to \infty$. The proportion of energy transmitted T will be a nontrivial function of the dune's geometry and of the ratios of densities and seismic velocities between the dune and the desert floor, as governed by the Zoeppritz equations *Zoeppritz* [1919]; *Aki and Richards* [1980]. For a given dune, T will be determined by the direction of arrival $\hat{\mathbf{r}}_{SD}$, governing the geometry encountered by the incident surface-wave, and f, governing the distribution with depth of the incident surface wave energy.

We assume that, once transmitted to the dune, the wave packet loses coherence, so that the seismic energy adopts a distribution among the available degrees of freedom that is independent of initial conditions. In this state, a constant proportion of energy will be lost over time to transmission through the dune's boundary, resulting in an exponential decay of energy density within the dune. Without attenuation, the decay timescale τ will be a nontrivial function of density and velocity ratios, but also of the distribution of energy within the dune and hence of f. The dune will support a spectrum of normal modes, at which resonance will be achieved and τ will be significantly larger. Having units of time, we expect τ to scale with the timescale of energy propagation between internal reflections $L/\langle c \rangle_D$, for $\langle c \rangle_D$ a typical seismic velocity within the dune. Given this decay timescale, the total energy within the dune, at time t, will be

$$E_D(t) \approx \frac{E_S L T(\hat{\mathbf{r}}_{SD}, f)}{2\pi||\mathbf{r}_{SD}||} \exp\left[\frac{1}{\tau(f)}\left(t_S + \frac{||\mathbf{r}_{SD}||}{c_R} - t\right)\right]. \tag{2}$$

Being conserved, any energy lost in the dune will be emitted, propagating to the far field with a geometry, density, velocity and frequency-dependent radiation pattern. We expect again the preponderance of energy to be transmitted by surface waves, and so write $D(\mathbf{n})\mathrm{d}\theta/2\pi$ for the proportion of energy propagated to the far field within angle element $\mathrm{d}\theta$ about horizontal direction $\mathbf{n}$. As a result, at a distant receiver location $\mathbf{x}_R = \mathbf{x}_D + \mathbf{r}_{DR}$ and at time $t > t_S + ||\mathbf{r}_{SD}||/c_R + ||\mathbf{r}_{DR}||/c_R$, the energy flux of arriving scattered surface waves, per unit distance in the azimuthal direction, will be given by

$$\mathscr{F} \approx \frac{E_S L T(\hat{\mathbf{r}}_{SD}, f) D(\hat{\mathbf{r}}_{DR}, f)}{4\pi^2||\mathbf{r}_{SD}||||\mathbf{r}_{DR}||\tau(f)} \exp\left[\frac{1}{\tau(f)}\left(t_S + \frac{||\mathbf{r}_{SD}||}{c_R} + \frac{||\mathbf{r}_{DR}||}{c_R} - t\right)\right]. \tag{3}$$

The resulting amplitude of vertical displacement was given by *Rose* [1984]. Dependence on dune geometry and the ratios of densities and seismic velocities is neglected in the above argument, but will enter into T, D and τ.

3 Model validation

3.1 Validation of assumptions

To examine the above assumptions, and to quantify T, D, and τ, we analyze synthetic seismograms generated in further numerical simulations. Using the barchan dune model depicted in Figure 1c, we conduct simulations of four delta-function point forces, with positions illustrated in Figure 4a. We consider the system's response to sources localized about time $t = 0$ and about frequencies f_0, by convolving synthetic seismograms with Gabor wavelets, waveforms

$$F(t) = \exp(-f_0^2 t^2/4)\exp(2\pi i f_0 t). \tag{4}$$

These wavelets provide optimum time-frequency localization, in the sense of minimizing the product of time-domain and frequency-domain standard deviations. We approximate E_S in frequency space for each f_0, assuming surface forcing and using the work of *Miller and Pursey* [1955], and take L to be the distance between the horns, equal to 200 m. We first analyze displacements at locations below the dune's brinkline, to consider the increase and decay of energy density within the dune.

In accordance with our model, the transmission of energy to the dune is associated with the arrival of Rayleigh waves, and the subsequent decay of energy within the dune E_D is exponential (Figure 4b). We infer this from the exponential decay of the more easily-measured energy density, $U = E_D/V$ for dune volume V, and conduct a least-squares best linear fit of $\ln(U)$ against t at each receiver within this dune. Using this regression and calculating constants E_S from the source waveform, L, $\mathbf{r}_{SD}$ and V from the simulated geometry, and c_R from the cubic equation for Rayleigh wave speed, we extract transmission and decay constants T and τ.

Extracted transmission and decay constants T and τ scale appropriately with dune size and with seismic velocities within the dune (Figure 4c). In particular, T increases with source frequency, as Rayleigh wave energy is increasingly concentrated close to the surface, before decreasing sharply as self-interference at arrival becomes significant. Superimposed on these general trends are smaller variations, which we associate with the varying proportion of wave energy emitted as the wavepacket loses coherence within the dune. Dependence of T on the direction of arrival is complex, corresponding to the non-trivial geometry encountered, with the range of variation approximately one order of magnitude. τ, meanwhile, is independent of the direction of arrival, indicating that the late-time distribution of energy within the dune is indeed independent of initial conditions. τ is of the same order as the timescale for shear wave propagation between internal reflections, and has a distinct peak corresponding to resonance, as suggested by *Levander* [1990], and as discussed in the case of subsurface heterogeneities by *Korneev* [2009]. We hypothesize that this 'resonant frequency' is associated with a wavelength of shear waves within the dune equal to the typical vertical thickness of the dune, $H/2$. Having established the values of parameters T and τ, equation 2 specifies the energy inside the dune over time and hence the rate at which it emits energy.

To investigate the transmission of energy emitted by the dune, we analyze synthetic seismograms in the far field, generated in the same simulations but corresponding now to surface locations a) at increasing radial distance from the dune center, in the same direction, and b) at a constant radial distance of 180 m from the dune's center and arranged around it. We again use the Gabor wavelets specified by equation 4. As expected, Rayleigh waves are predominantly responsible for transmitting energy to the far field, as demonstrated by the characteristic propagation velocity and elliptical displacement

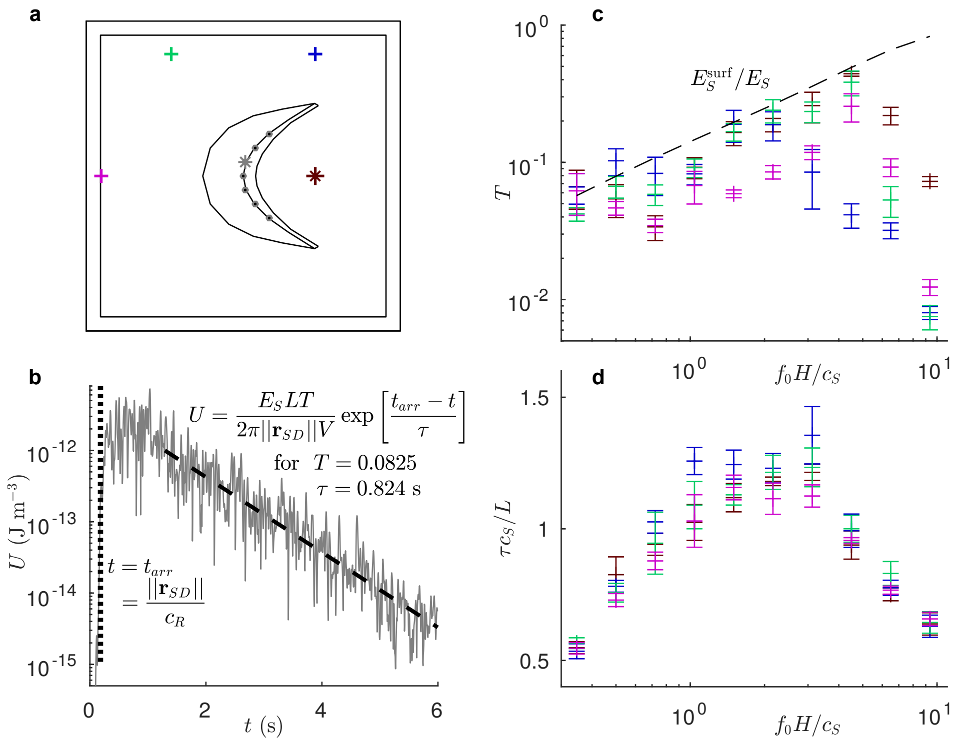

Figure 4. Energy decay within the dune, agreeing with our simplified model. **a**) Locations of simulated sources (+) and receivers (•). Receivers are at the level of the desert floor. **b**) Example of the decay of energy density U within the dune, of volume V, for the source and receiver marked $*$, with the source waveform being a Gabor wavelet of center frequency 168 Hz. U increases sharply at a time associated with Rayleigh wave arrival, adjusts over a timescale of approximately 1 s, and then decays exponentially. Decay constants T and τ are extracted by a least-squares best linear fit of $\ln(U)$ against t, and calculated given constants E_S, L, $||\mathbf{r}_{SD}||$, c_R, and dune volume V. **c** and **d**) Decay constants T and τ, respectively, as functions of source wavelet center frequency f_0. Colors correspond to sources in **a**, while error bars correspond to standard error over the seven simulated receivers. We non-dimensionalize with dune height H, lateral size L, and shear velocity c_S, and the dashed line indicates the proportion $E_S^{\rm surf}/E_S$ of Rayleigh wave energy above a depth of 1 m, acting as an upper bound for T. T varies by up to an order of magnitude with source position, and decreases rapidly at higher f_0. τ is independent of source position, is of the same order as L/c_S, and is peaked at a frequency corresponding to shear wave resonance across half the height H of the dune.

trajectories shown in Figure 5a. We calculate the relative Rayleigh wave energy flux at simulated receivers to extract directivities D, which are plotted in Figure 5b.

3.2 Verification of predictions

Having established the fundamental assumptions of our mathematical model, and extracted its parameters, we compare its predictions of ground-roll noise level with observations from simulations. We conduct a simulation with realistic receiver line in the vicinity of a dune, as depicted schematically in Figure 6a, and produce a synthetic seismogram (Figure 6b) in which the expected features can be observed: a direct Rayleigh wave, initial reflections from the dune, and subsequent arrivals of waves emitted from the dune following absorption and reverberation.

In Figure 6c, we compare the observed receiver displacements due to the latter to the amplitudes predicted by our model, and note that our predictions represent a remarkably tight bound, over the entire receiver line and over a time in which the energy flux of passing waves decreases by a factor of 400. The only exception to this corresponds to waves emitted from the dune at early times (after a residence time within the dune of ≈ 0.4 s), when energy within the dune has not yet adopted a distribution independent of initial conditions. Over a duration of ≈ 0.4 s at each receiver, a coherent wavepacket passes receivers upwind of the dune, after having travelled through the dune, been reflected from its leeward face, and travelled back. Even at these times, the bounds established by our model are exceeded by a factor of only three.

4 Exploration of parameter space

4.1 Dune geometry

Whilst we have established our model's accuracy for the mesh hitherto discussed, its applicability to physical scenarios depends on the stability of its parameters to changes in dune geometry. We therefore examine the sensitivity of the parameters T, τ, and D to changes in dune length, width, and height. Specifically, we construct new meshes, each including a dune with the same hyperbolic crest line and angled faces discussed in Section 2.2, but with, in turn and with all else held constant in each case: length X increased by a factor of 1.6; width Y increased by a factor of 1.5; and height H reduced by a factor of 2. While these parameter values are unrealistic, they may be thought of as exag-

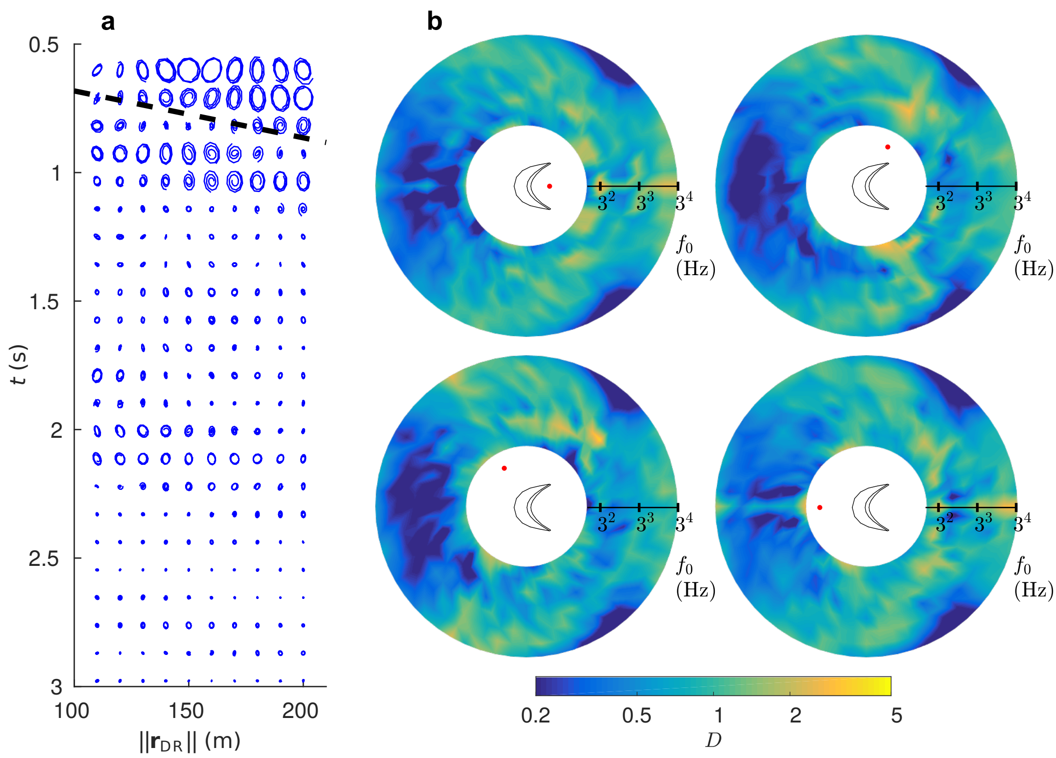

Figure 5. Energy emission to the far field. **a**) Illustrative hodogram of the real component of displacement for a source 100 m downwind of the dune's centre and with a Gabor wavelet waveform of center frequency 27 Hz. The direction from the dune's center to receivers is at 90° to the wind, and subplots are particle paths in the radial-vertical plane, over 0.11 s time windows. The dashed line indicates the Rayleigh wave propagation speed. Particles trace the elliptical trajectories characteristic of Rayleigh waves, and disturbances propagate radially outwards at the Rayleigh wave velocity. **b**) Directivity D for varying source positions • relative to the dune. For each source position, we consider 60 receivers, each 180 m from the dune's center and with an azimuthal separation of 6° from its neighbours. We measure at each receiver, position $180\mathbf{n}$ relative to the dune's center, the square amplitude $A(\mathbf{n}, t; f_0)$ of vertical displacement, in response to a source with a Gabor wavelet waveform of center frequency f_0. We define $D(\mathbf{n}, f_0)$ as the median over late times, after the direct wave and initial reflections have passed, of $A(\mathbf{n}, t; f_0)/\langle A(\mathbf{n}, t; f_0)\rangle_{\mathbf{n}}$, and represent D by color in radial plots, with azimuth corresponding to that of $\mathbf{n}$ and radial distance to f_0. We observe that D is only weakly dependent on the source's position, as assumed by our model, and that D varies by over an order of magnitude, with little energy emitted upwind of the dune at a wide range of frequencies, or in the direction of the horns at high frequencies.

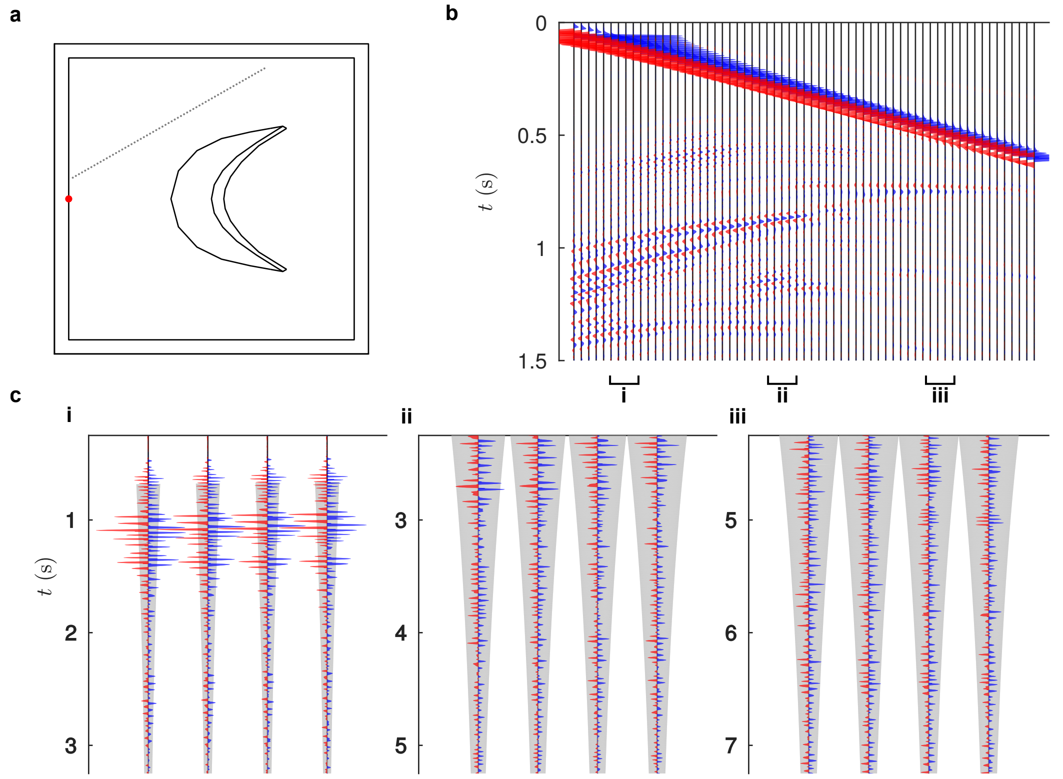

Figure 6. Verification of predictions. **a**) Locations of simulated source (●) and receivers (·). The source waveform is a Ricker wavelet of center frequency $f_0 = 20$ Hz, and the receivers are at the level of the desert floor with 5 m spacing between them. **b**) Synthetic seismogram, showing vertical displacement at the receiver locations, over time. The direct Rayleigh wave is at the top of the record, while the first arrivals of waves reflected from and emitted by the dune are at 0.5 s and 0.7 s, respectively. 12 receivers, in the three regions indicated by i, ii, and iii, are selected for model verification. **c**) Comparison of observed displacements (trace) to amplitudes predicted by equation 3 (gray envelope), for the receivers in regions i, ii, and iii. Parameter values are estimated by linear interpolation in $\log f_0$, $\arg \mathbf{r_{SD}}$, and $\arg \mathbf{r_{DR}}$, as appropriate. With the exception of the wave in i) arriving at $t = 1.1$ s, after a single internal reflection in the dune (for which the order of magnitude is correctly predicted), the model provides an excellent bound for displacement due to energy emitted from the dune, over a range of receivers and a factor 20 decrease in displacement magnitude over time.

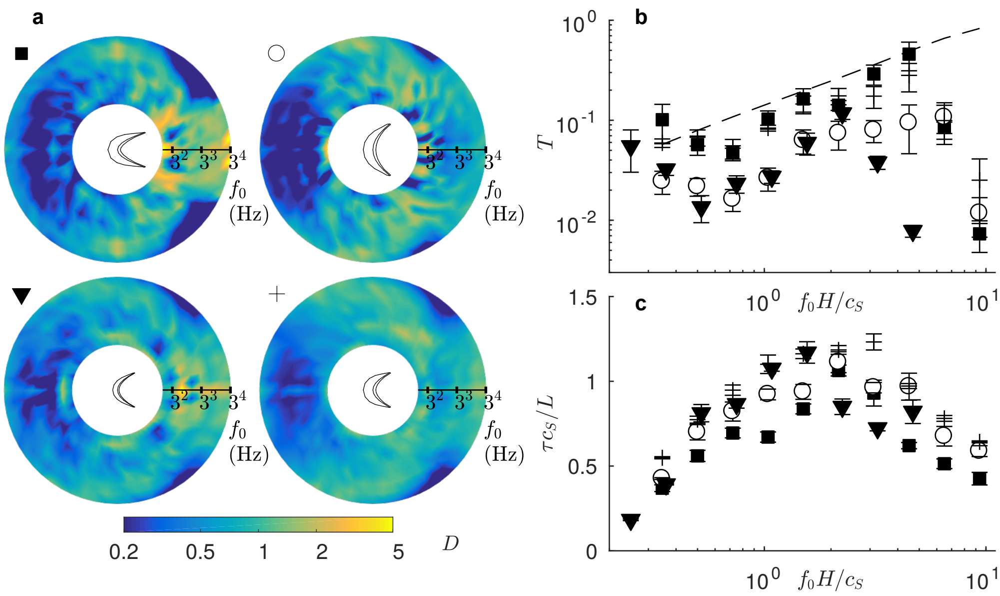

Figure 7. Parameter variation in the case of long (■, X = 160), wide (○, Y = 150), and short (▼, H = 5) dunes, as compared to the dune described in previous sections (+, X = Y = 100, H = 10). **a**) Variation of directivity D, calculated as described in Figure 5b. In the center of each subplot is a schematic of the corresponding dune geometry. **b** and **c**) Variation of T and τ, respectively, calculated as described in Figure 4c.

gerations of reasonable, realistic variations within the parameter space. We use the same methods to determine parameter values as described in Section 3.1, with the source 100 m downwind of the dune crest, except that we now define $L = 2\sqrt(XY)$, consistent with the above but taking into account the length of the dune's horns.

Figure 7 demonstrates that the model parameters display similar behavior over a wide range of dune geometries. T, τ, and D vary under changes of X, Y, and H, but the magnitude of such variation is typically less than that achieved by a proportionate change in $\arg \mathbf{r_{SD}}$, f_0, or $\arg \mathbf{r_{DR}}$. In addition, not only are the parameters of the same order as predicted in Section 2.3 and measured in Section 3.1, but the frequency corresponding to resonance in the dune is approximately $2c_s/H$ for all dune geometries considered, as previously hypothesized.

4.2 Internal structure

Thus far, we have considered a highly simplified model of seismic velocities, assuming homogeneity in the desert floor and homogeneity within the dune. For the sake of continued simplicity and, in particular, so that Rayleigh waves remain non-dispersive, we maintain the assumption of homogeneity within the desert floor, with density 2500 kg m^{-3}, $c_P^f = 1000$ m s^{-1}, and $c_S^f = 600$ m s^{-1}. However, to investigate whether dunes' internal structure has a significant effect on their absorption and re-emission of ground roll, we now consider a more realistic model for the dune, and allow seismic velocities to vary throughout its volume.

We use models for density and seismic velocities within the dune derived from existing literature, with the intention of calculating physically reasonable distributions of these quantities. On the basis of *Logie* [1981] and *Ritsema and Dekker* [1994], we take the bulk density throughout the dune to be 1600 kg m^{-3}. We assume pressure p to be lithostatic and use the empirical models proposed by *Bodet et al.* [2014] for seismic velocities in dry sand, with $c_P^{\text{dry}} = 21p^{0.30}$ and $c_S^{\text{dry}} = 8.2p^{0.33}$, for quantities measured in SI units. To include the effect of water saturation, as found to be significant by *Vriend et al.* [2015], we use the results of *Barrière et al.* [2012] and assume that seismic velocities decrease by 0.2% of their dry values for each 1% increase in water saturation, hence 0.5% of their dry values for each 1% increase in water content by volume. We suppose that within the dune, with upwind distance from the dune's slip face, 12 m thick layers in which water content by volume is 1.2% alternate with 4 m thick layers in which water content by volume is 6%. This corresponds to 9-month 'dry' seasons being followed by 3-month 'wet' seasons, for a dune migrating at a constant velocity of 16 m yr^{-1}; these conditions may be considered a physically reasonable idealization of those observed by *Louge et al.* [2013] and *Berndtsson et al.* [1996]. Under these assumptions, seismic velocities within the dune will have the distributions represented in Figure 8a. We write $\langle c_S \rangle$ for the mean shear wave velocity within the dune.

Given this velocity structure, and the mesh geometry discussed in Section 2.2, we simulate a point force 100 m downwind of the dune's crest and extract parameters T, τ, and D as described in Section 3.1. The resulting parameter values are shown in Figures 8b and 8c.

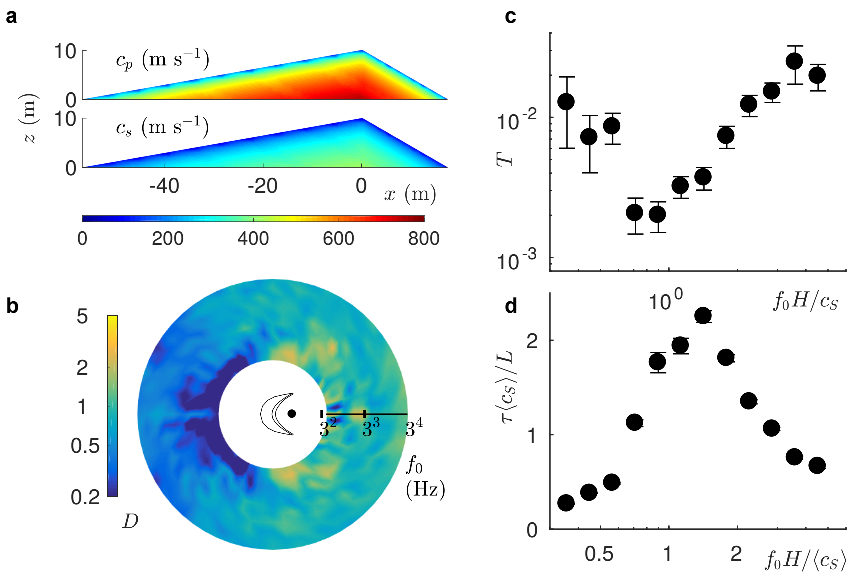

Figure 8. Parameter values in the case of internal structure. **a**) Velocity model in the $y = 0$ section through the dune's centerline. **b**) Values of directivity D, calculated as described in Figure 5b. **c** and **d**) Values of T and τ, respectively, calculated as described in Figure 4c. We non-dimensionalize as previously, but now with $\langle c_S \rangle = 280$ m s^{-1}, the mean shear wave velocity within the dune.

Model parameters have similar behavior to that noted in the case of a homogeneous dune, but differ significantly in their exact values. In Figure 8b, T is measured to be approximately an order of magnitude lower than in the case of a homogeneous dune, with the majority of the energy absorbed by the dune re-emitted before the adoption of a time-independent distribution. However, T demonstrates the same increase with f_0 as previously noted, and the same decrease at high f_0. Similarly, τ demonstrates the same resonance-associated peak at $f_0 \approx 2\langle c_S \rangle/H$, but we note that the peak is significantly narrower and, when suitably non-dimensionalized, higher, indicating a stronger resonance. Considering D, Figure 8c demonstrates preferential energy emission in the direction of the dune's migration, as observed for a homogeneous dune. However, even at the highest center frequencies investigated we observe no deficit in the energy emitted in the direction of the dune's horns, and this is markedly contrary to results in the homogeneous case.

5 Discussion and conclusions

We have demonstrated that, under reasonable physical assumptions, an isolated barchan sand dune will be a significant source of off-line scattered ground roll over a prolonged interval of time, as a result of the absorption and subsequent re-emission of seismic energy. As depicted in the movies in supplemental material, a significant proportion of the energy radiated by a seismic source will propagate in the form of Rayleigh waves, or ground roll, and some proportion of the energy reaching a dune will be transmitted through its boundary and absorbed by its interior. Internal reflection will lead to reverberation of this energy within the dune, with some proportion transmitted through the dune's boundary in each interval of time. It is this re-emitted energy, propagating to the receiver spread in the form of Rayleigh waves, that will manifest itself as noise in seismometer traces.

We have developed and verified a simple analytical model for the process of energy absorption and re-emission, providing a tight bound on the amplitude of noise due to re-emitted ground roll. Our assumptions, that Rayleigh waves are the dominant mechanism for energy transfer and that the energy absorbed by the dune quickly adopts a distribution independent of initial conditions, imply that energy density within the dune will display a characteristic sudden increase and exponential decay, which we observed in our simulations. Using one set of simulations to extract parameters of our analytical model, we verified that they take physically reasonable values, and successfully predicted the amplitude of noise at a realistic receiver spread in an independent simulation.

Under variations of dune geometry and internal structure, we have shown that the model's parameters have similar behaviour, estimable from easily-measurable properties of the dune such as height H, typical width L and typical shear wave velocity c_S. The proportion T of arriving energy transmitted to the dune increases with the typical frequency of the source's oscillations f_0, associated with the increasing proportion of the Rayleigh wave energy concentrated near the surface, before decreasing as self-interference becomes significant at $f_0 \sim c_S$. The decay time τ has a peak at $f_0 \approx 2c_S/H$, attaining a value $\tau \approx L/c_S$, associated with a half-height shear wave resonance within the dune, and decreases for greater and lesser f_0. Of the energy emitted from the dune, a lower proportion D is directed upwind of the dune, away from its horns, than is emitted in the direction of the dune's horns.

Our results allow quantitative predictions of the seismic noise arriving at surficial receivers in the vicinity of an isolated barchan, which can be validated in field experiments. Field data can be examined for evidence of scattered ground roll arrivals associated with isolated barchan dunes, and for exponential decay of the amplitude of the noise associated with these arrivals.

For the sake of simplicity, some physical properties that are significant in the field have been neglected. In particular, we neglected attenuation, assumed constant seismic velocities in the desert floor, and assumed a single dune rather than considering multiple dunes. Neglecting attenuation will have a significant effect on the amplitude of dune-scattered ground roll, since uncohesive sand is strongly attenuative. However, isotropic anelastic attenuation may easily be added to our work by adding a multiplicative term to our analytic model, of the form $\exp\left[-\pi f(t_{SD} + t_{DR})/Q^f\right] \exp\left[-\pi f(t - t_{SD} - t_{DR})/Q\right]$ for seismic quality factor Q^f in the desert floor and Q in the dune. Assuming constant seismic velocities in the desert floor will significantly change the arrival time of dune-scattered ground roll, since Rayleigh waves are dispersive in a heterogeneous medium, and the near surface is typified by significant increases in seismic velocity with depth. However, the effect of this change may also be included, by replacing the constant Rayleigh wave velocities in our analytic model with the frequency-dependent Rayleigh wave velocities of the region with which one is concerned. Finally, the effect of multiple dunes may be considered by considering the energy flux arriving at a receiver and conducting a perturbation expansion, in the geometric attenuation factor between dunes, analogous to that used for multiple scatterers. To first order in this factor, the contributions of each dune may be considered in isolation, and summed to calculate the total contribution of the dune field. To second order, each dune radiating ground roll must be considered as a source in relation to each other dune, and the related contributions again summed. Continuing this process would yield a noise estimate that takes into account an arbitarily large number of inter-dune interactions, making the effect of a dune field calculable.

Of perhaps more concern, a number of the properties we have used are poorly quantified in the field. The estimates used for seismic velocities within sand dunes are drawn from a limited number of studies, none of which have probed the entire depth of a barchan dune. Extrapolating the results of laboratory studies to the field, as we did in the case of seismic velocities' dependence on pressure and on water saturation in Section 4.2, is prone to error, and the results are often in conflict with data from the field. For example, *Barrière et al.* [2012] suggested that seismic velocities should decrease with increasing water content, contrary to the observations of *Vriend et al.* [2015].

However, given better quantification of system parameters, or the validation in the field of predictions made with existing estimates of such parameters, our work implies the possibility of tailoring survey design to minimise the deleterious effects of dune-scattered ground roll. The work we have presented suggests that, to minimise noise, receivers are best placed upwind of isolated barchan dunes, and that, in the vicinity of a dune of height H and typical shear wave velocity c_S, frequencies $f_0 \approx 2c_S/H$ are best avoided in analysis. Equation 3 also allows the establishment of a criterion for the necessary distance from a given dune to detect a signal of specified arrival time and amplitude, in a specified frequency range of analysis.

A: Mesh refinement study

We verify the numerical accuracy of our simulations by a mesh refinement study on a quasi-2D model of a transverse dune, with profile given by the midline of our original barchan dune model. The mesh geometry, shown in Figure A.1a, is 200 m long, 200 m wide, and 70 m deep, with CPML 25 m thick on each side and 30 m deep at its base. The dune geometry is defined by a straight brinkline along the mesh's center, at a height of $H = 10$m, and by constant slope angles on the windward and leeward faces of 10° and 30° respectively. Velocities of the P and S waves are 1000 and 600 m s^{-1} in the desert floor, and 350 and 180 m s^{-1} in the dune. Density is everywhere 2500 kg m^{-3}. We simulate point forces 50 m upwind of, below, and 50 m downwind of the brinkline, acting vertically 1 m below the surface with Ricker function waveforms, central frequency 10 Hz and amplitude 10^5 N. Synthetic seismograms are recorded along a surface receiver line on the desert floor, transverse to the crest, with sources 50 m offline. The simulation duration is 2.4 s.

Varying the interval between mesh points δx, with a proportionate time step, we find that error in displacement decays as $\delta x^{2.9\pm0.3}$, with $\delta x = H/2$ sufficient for 10% accuracy. An example of the convergence of simulated displacement is shown in Figure A.1b, with the decay of mean squared error in displacement depicted in Figure A.1c.

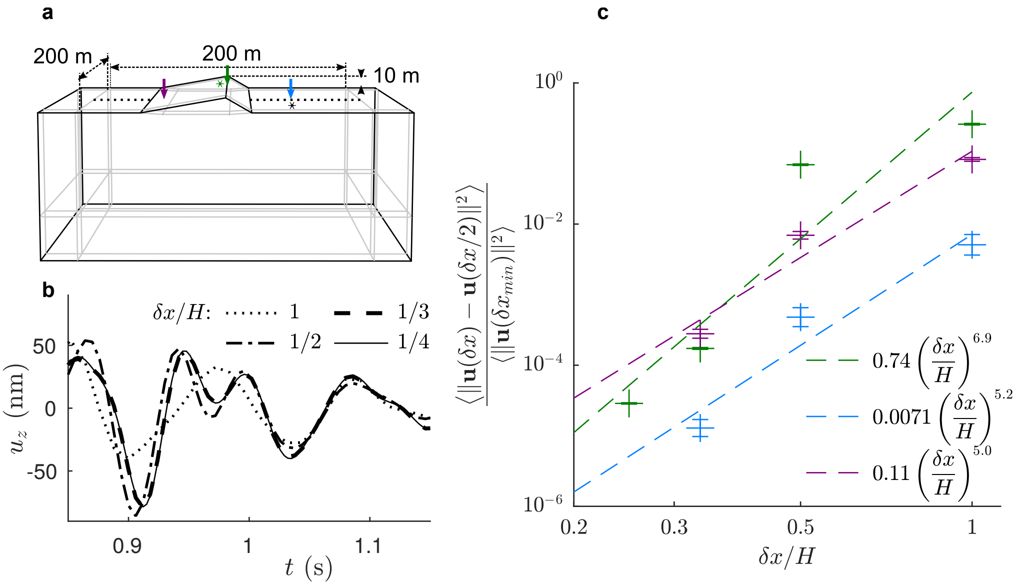

Figure A.1. Numerical convergence in a quasi-2D model. **a**) Geometry used for mesh-refinement study. Simulated sources are at locations ↓, with a burial of 1 m, while receivers are the surface at locations ▪. **b**) Convergence of simulated displacement for the source receiver pair marked by $*$ in **a**, for decreasing $\delta x/H$. **c**) Decay, with decreasing interval between mesh points δx, of the mean over time t of squared error in simulated displacement $\mathbf{u}(t; \delta x)$. We normalize by our best estimate of mean squared displacement. Colors correspond to the source locations in **a**, while error bars are the standard error over the 26 receiver locations.

B: Assessment of CPML efficiency

We assess the efficiency of our convolutional perfectly-matched boundary layers (CPML) by comparing our simulations to analytic solutions in the case of a point force on a homogeneous halfspace. We use a mesh 400 m long, 400 m wide, and 100 m deep, with typical mesh spacing 5 m and CPML 4 grid points thick on each side, and with constant velocities of P and S waves, 1000 m s^{-1} and 600 m s^{-1}, respectively. We simulate a vertical point force 100 m downwind of the center of the mesh's surface, at a depth of 1 m and with a delta function waveform, and consider receiver locations at the surface, 180 m from the center and at 5° azimuthal intervals. The duration of the simulation is 6 s. We convolve synthetic seismograms with Gabor wavelets, as specified by equation 4 with center frequencies from $f_0 = 6$ Hz to $f_0 = 81$ Hz, and calculate the total energy flux $J_{\text{obs}}(\mathbf{x}_R, f_0)$ past each receiver location for each center frequency. We compare the results to the analytically-derived net energy fluxes for Rayleigh waves, in the same situation, in the cases of a) perfectly-absorbing boundaries ($J_{\mathrm{abs}}(\mathbf{x}_R, f_0)$ and of b) perfectly-reflecting boundaries ($J_{\mathrm{ref}}(\mathbf{x}_R, f_0)$), using the work of *Miller and Pursey* [1955] and *Rose* [1984] and the method of images in the case of b).

Since Rayleigh waves dominate the signal received at the simulated receivers, a tight overestimate of the total reflected energy flux is given by $J_{\mathrm{obs}} - J_{\mathrm{abs}}$, and a tight underestimate of the worst-case total reflected energy flux is given by $J_{\mathrm{ref}} - J_{\mathrm{abs}}$. Our lower bound for the efficiency of our CPML is therefore $1 - (J_{\mathrm{obs}} - J_{\mathrm{abs}})/(J_{\mathrm{ref}} - J_{\mathrm{abs}})$, and we find that at no receiver, and at no center frequency analysed, does this fall below 99%.

Acknowledgments

This work was supported by the National Environmental Research Council [grant number NE/L002507/1]; the Royal Society [grant number DH120121]; and the Schlumberger Gould Research Centre. At the Schlumberger Gould Research Centre, we gratefully acknowledge the support of Ed Kragh and Jon-Fredrik Hopperstad for this project.

No new geophysical data were used in producing this manuscript.

References

Aki, K., and P. Richards (1980), *Quantitative Seismology: Theory and Methods*, no. v. 1 in A Series of books in geology, W. H. Freeman.

Al-Dabi, H., M. Koch, M. Al-Sarawi, and F. El-Baz (1997), Evolution of sand dune patterns in space and time in north-western Kuwait using Landsat images, *Journal of Arid Environments*, *36*(1), 15–24, doi:10.1006/jare.1996.0230.

Almalki, H., and T. Alkhalifah (2012), Mapping the base of sand dunes using a new design of land-streamer for static correction applications, *Journal of Petroleum Exploration and Production Technology*, *2*(2), 57–65, doi:10.1007/s13202-012-0022-1.

Ashour, M. M. (1987), Surficial deposits of Qatar Peninsula, *Geological Society, London, Special Publications*, *35*(1), 361–367, doi:10.1144/GSL.SP.1987.035.01.24.

Bagnold, R. A. (1941), *The Physics of Blown Sand and Desert Dunes*, Methuen.

Barrière, J., C. Bordes, D. Brito, P. Sénéchal, and H. Perroud (2012), Laboratory monitoring of P waves in partially saturated sand, *Geophysical Journal International*, *191*(3), 1152–1170, doi:10.1111/j.1365-246X.2012.05691.x.

Berndtsson, R., K. Nodomi, H. Yasuda, T. Persson, H. Chen, and K. Jinno (1996), Soil water and temperature patterns in an arid desert dune sand, *Journal of Hydrology*, *185*(1), 221–240, doi:10.1016/0022-1694(95)02987-7.

Bishop, M. A. (2013), Dune field development, interactions and boundary conditions for crescentic and stellate megadunes of the Al Liwa Basin, the Empty Quarter, *Earth Surface Processes and Landforms*, *38*(2), 183–191, doi:10.1002/esp.3318.

Bodet, L., A. Dhemaied, R. Martin, R. Mourgues, F. Rejiba, and V. Tournat (2014), Small-scale physical modeling of seismic-wave propagation using unconsolidated granular media, *GEOPHYSICS*, *79*(6), T323–T339, doi:10.1190/geo2014-0129.1.

Bourbi´, T., O. Coussy, and B. Zinszner (1987), *Acoustics of Porous Media*, *The Rock Physics Handbook: Tools for Seismic Analysis of Porous Media*, Institut français du pétrole publications, Gulf Publishing Company.

Bristow, C., J. Pugh, and T. Goodall (1996), Internal structure of aeolian dunes in Abu Dhabi determined using ground-penetrating radar, *Sedimentology*, *43*(6), 995–1003, doi:10.1111/j.1365-3091.1996.tb01515.x.

Chen, Y., S. Jiao, J. Ma, H. Chen, Y. Zhou, and S. Gan (2015), Ground-Roll Noise Attenuation Using a Simple and Effective Approach Based on Local Band-Limited Orthogonalization, *IEEE Geoscience and Remote Sensing Letters*, *12*(11), 2316–2320, doi:10.1109/LGRS.2015.2475280, cited By 2.

Combee, L. (1994), Wavefield Scattering By a 2-D Near-surface Elliptic Anomaly, *1994 SEG Annual Meeting, 23-28 October, Los Angeles, California.*

Cordsen, A., and M. Galbraith (2002), Narrow- versus wide-azimuth land 3D seismic surveys, *The Leading Edge*, *21*(8), 764–770, doi:10.1190/1.1503181.

Criswell, D. R., J. F. Lindsay, and D. L. Reasoner (1975), Seismic and acoustic emissions of a booming dune, *Journal of Geophysical Research*, *80*(35), 4963–4974, doi:10.1029/JB080i035p04963.

Dincer, T., A. Al-Mugrin, and U. Zimmermann (1974), Study of the infiltration and recharge through the sand dunes in arid zones with special reference to the stable isotopes and thermonuclear tritium, *Journal of Hydrology*, *23*(1), 79–109, doi:10.1016/0022-1694(74)90025-0.

Dong, S., R. He, and G. T. Schuster (2006), *Interferometric prediction and least squares subtraction of surface waves*, SEG Technical Program Expanded Abstracts 2006 pp. 2783–2786, doi:10.1190/1.2370102.

Drummond, J. M., R. Kasmi, A. Sakani, A. J. L. Budd, and J. W. Ryan (2003), Optimizing 3-D seismic technologies to accelerate field development in the Berkine Basin, Algeria, *Geological Society, London, Special Publications*, *207*(1), 257–273, doi:10.1144/GSL.SP.2003.207.13.

Duffy, J., and R. Mindlin (1956), *Stress-strain Relations and Vibrations of a Granular Medium*, Defense Technical Information Center.

El-Sayed, M. (2000), The nature and possible origin of mega-dunes in Liwa, Ar Rub' Al Khali, {UAE}, *Sedimentary Geology*, *134*(3–4), 305–330, doi:10.1016/S0037-0738(00)00052-X.

Embree, P., J. P. Burg, and M. M. Backus (1963), Wide-band velocity filtering; The Pie-Slice process, *Geophysics*, *28*(6), 948–974, doi:10.1190/1.1439310.

Finkel, H. J. (1959), The Barchans of Southern Peru, *The Journal of Geology*, *67*(6), 614–647.

Flinn, E. (1965), Signal Analysis Using Rectilinearity and Direction of Particle Motion, *Proceedings of the IEEE*, *53*(12), 1874–1876, doi:10.1109/PROC.1965.4462, cited By 107.

Fontes, J., M. Yousfi, and G. Allison (1986), Estimation of long-term, diffuse groundwater discharge in the northern Sahara using stable isotope profiles in soil water, *Journal of Hydrology*, *86*(3), 315–327, doi:10.1016/0022-1694(86)90170-8.

Forghani, F., and R. Snieder (2010), Underestimation of body waves and feasibility of surface-wave reconstruction by seismic interferometry, *The Leading Edge*, *29*(7), 790–794, doi:10.1190/1.3462779.

Gercek, H. (2007), Poisson's ratio values for rocks, *International Journal of Rock Mechanics and Mining Sciences*, *44*(1), 1–13, doi:10.1016/j.ijrmms.2006.04.011.

Geuzaine, C., and J.-F. Remacle (2009), Gmsh: a three-dimensional finite element mesh generator with built-in pre- and post-processing facilities, *International Journal for Numerical Methods in Engineering*, *79*(11), 1309–1331.

Halliday, D., P. Bilsby, L. West, E. Kragh, and J. Quigley (2015), Scattered ground-roll attenuation using model-driven interferometry, *Geophysical Prospecting*, *63*(1), 116–132, doi:10.1111/1365-2478.12165.

Halliday, D. F., A. Curtis, P. Vermeer, C. Strobbia, A. Glushchenko, D.-J. van Manen, and J. O. A. Robertsson (2010), Interferometric ground-roll removal: Attenuation of scattered surface waves in single-sensor data, *Geophysics*, *75*(2), SA15–SA25, doi:10.1190/1.3360948.

Hardin, B. O., and W. L. Black (1968), Vibration Modulus of normally consolidated Clay, *J. Soil Mech. Found. Div., ASCE*, *95*(SM2), 353–369.

Holm, D. A. (1960), Desert Geomorphology in the Arabian Peninsula, *Science*, *132*(3437), 1369–1379, doi:10.1126/science.132.3437.1369.

Hu, Y., L. Wang, F. Cheng, Y. Luo, C. Shen, and B. Mi (2016), Ground-roll noise extraction and suppression using high-resolution linear Radon transform, *Journal of Applied Geophysics*, *128*, 8–17, doi:10.1016/j.jappgeo.2016.03.007.

Hudson, J. A., and L. Knopoff (1967), Statistical properties of Rayleigh waves due to scattering by topography, *Bulletin of the Seismological Society of America*, *57*(1), 83–90.

Jackson, G. M., I. M. Mason, and S. A. Greenhalgh (1991), Principal component transforms of triaxial recordings by singular value decomposition, *Geophysics*, *56*(4), 528–533, doi:10.1190/1.1443068.

Janssen, H. A. (1895), Experiments on Corn Pressure in Silo Cells, *Zeitschr. d. Vereines deutscher Ingenieure*, *39*, 1045.

Jawad Ali, A., and R. A. Al-Ani (1983), Sedimentological and geomorphological study of sand dunes in the Western Desert of Iraq, *Journal of Arid Environments*, *6*(1), 13–32.

Kirchheimer, F. (1985), *On some further aspects of fan filtering*, SEG Technical Program Expanded Abstracts 1985 pp. 635–638, doi:10.1190/1.1892782.

Komatitsch, D., and R. Martin (2007), An unsplit convolutional Perfectly Matched Layer improved at grazing incidence for the seismic wave equation, *GEOPHYSICS*, *72*(5), SM155–SM167, doi:10.1190/1.2757586.

Komatitsch, D., J. Ritsema, and J. Tromp (2002), The Spectral-Element Method, Beowulf Computing, and Global Seismology, *Science*, *298*(5599), 1737–1742, doi:10.1126/science.1076024.

Korneev, V. (2009), Resonant seismic emission of subsurface objects, *GEOPHYSICS*, *74*(2), T47–T53, doi:10.1190/1.3068448.

Kragh, E., and L. Peardon (1995), Ground roll and polarization, *First Break*, *13*(9), 369–378, cited By 5.

Lancaster, N. (1982), Dunes on the skeleton coast, Namibia (South West Africa): Geomorphology and grain size relationships, *Earth Surface Processes and Land-*

forms, *7*(6), 575–587, doi:10.1002/esp.3290070606.

Levander, A. R. (1990), Seismic scattering near the earth's surface, *pure and applied geophysics*, *132*(1), 21–47, doi:10.1007/BF00874356.

Ling, Y., J. Gao, and R. Zhang (1998), Sand dune reverberation and its suppression, *The Leading Edge*, *17*(5), 697–702, doi:10.1190/1.1438043.

Logie, M. (1981), Wind tunnel experiments on dune sands, *Earth Surface Processes and Landforms*, *6*, 365–374, doi:10.1002/esp.3290060315.

Louge, M. Y., A. Valance, A. O. el Moctar, J. Xu, A. G. Hay, and R. Richer (2013), Temperature and humidity within a mobile barchan sand dune, implications for microbial survival, *Journal of Geophysical Research: Earth Surface*, *118*(4), 2392–2405, doi:10.1002/2013JF002839.

Mavko, G., T. Mukerji, and J. Dvorkin (2003), *The Rock Physics Handbook: Tools for Seismic Analysis of Porous Media*, Stanford-Cambridge program, Cambridge University Press.

McKee, E. D. (1979), A study of global sand seas, *Tech. rep.*

McKee, E. D. (1982), *Sedimentary structures in dunes of the Namib Desert, South West Africa*, Geological Society of America, Boulder, Colo.

Miller, G. F., and H. Pursey (1955), On the Partition of Energy between Elastic Waves in a Semi-Infinite Solid, *Proceedings of the Royal Society of London A: Mathematical, Physical and Engineering Sciences*, *233*(1192), 55–69, doi:10.1098/rspa.1955.0245.

Neal, A. (2004), Ground-penetrating radar and its use in sedimentology: principles, problems and progress, *Earth-Science Reviews*, *66*(3–4), 261–330, doi:10.1016/j.earscirev.2004.01.004.

Peter, D., D. Komatitsch, Y. Luo, R. Martin, N. Le Goff, E. Casarotti, P. Le Loher, F. Magnoni, Q. Liu, C. Blitz, T. Nissen-Meyer, P. Basini, and J. Tromp (2011), Forward and adjoint simulations of seismic wave propagation on fully unstructured hexahedral meshes, *Geophys. J. Int.*, *186*(2), 721–739, doi:10.1111/j.1365-246X.2011.05044.x.

Qian, R., J. Li, L. Liu, and Z. Zhao (2014), Internal Structure of Sand Dunes in the Badain Jaran Desert Revealed by GPR and Its Implications to Inter-Dune Lake Hydrology, pp. 166–169, 15th International Conference on Ground Penetrating Radar - GPR 2014, IEEE.

Regone, C. J. (1997), *11. Measurement and Identification of 3-D Coherent Noise Generated from Irregular Surface Carbonates*, Carbonate Seismology, pp. 281–306, doi:10.1190/1.9781560802099.ch11.

Richart, F. E., J. R. Hall, and R. D. Woods (1970), *Vibrations of soils and foundations*, Prentice-Hall international series in theoretical and applied mechanics, Prentice-Hall.

Ritsema, C. J., and L. W. Dekker (1994), Soil moisture and dry bulk density patterns in bare dune sands, *Journal of Hydrology*, *154*(1), 107–131, doi: 10.1016/0022-1694(94)90214-3.

Rose, L. (1984), On the energy radiated by Rayleigh waves, *Wave Motion*, *6*(4), 359–361, doi:10.1016/0165-2125(84)90038-6.

Schenk, C. J., D. L. Gautier, G. R. Olhoeft, and J. E. Lucius (2009), *Internal Structure of an Aeolian Dune using Ground-Penetrating Radar*, pp. 61–69, Blackwell Publishing Ltd., doi:10.1002/9781444303971.ch5.

Smid, J., and J. Novosad (1981), Pressure Distribution under Heaped Bulk Solids, *Proceedings of 1981 Powtech. Conference*, p. 63.

Tiapkina, O., M. Landrø, Y. Tyapkin, and B. Link (2012), Single-station SVD-based polarization filtering of ground roll: Perfection and investigation of limitations and pitfalls, *GEOPHYSICS*, *77*(2), V41–V59, doi:10.1190/geo2011-0040.1.

Tromp, J., D. Komatitsch, and Q. Liu (2008), Spectral-Element and Adjoint Methods in Seismology, *Communications in Computational Physics*, *3*(1), 1–32.

Vermeer, G. (2012), *3D Seismic Survey Design, Second Edition*, Society of Exploration Geophysicists, doi:10.1190/1.9781560803041.

Vriend, N., M. Hunt, R. Clayton, C. Brennen, K. Brantley, and A. Ruiz-Angulo (2007), Solving the mystery of booming sand dunes, *Geophysical Research Letters*, *34*(16), doi:10.1029/2007GL030276.

Vriend, N. M., M. L. Hunt, and R. W. Clayton (2015), Linear and nonlinear wave propagation in booming sand dunes, *Physics of Fluids*, *27*(10), 103,305, doi: 10.1063/1.4931971.

Walton, K. (1987), The effective elastic moduli of a random packing of spheres, *Journal of the Mechanics and Physics of Solids*, *35*(2), 213–226, doi:10.1016/0022-5096(87)90036-6.

Xu, X.-H., G.-Z. Qu, Y. Zhang, Y.-Y. Bi, and J.-J. Wang (2016), Ground-roll separation of seismic data based on morphological component analysis in two-dimensional domain, *Applied Geophysics*, *13*(1), 116–126, doi:10.1007/s11770-016-0546-0.

Yu, P., and F. E. Richart (1984), Stress Ratio Effects on Shear Modulus of Dry Sands, *Journal of Geotechnical Engineering*, *110*(3), 331–345, doi: 10.1061/(ASCE)0733-9410(1984)110:3(331).

Zhou, H. (2014), *Practical Seismic Data Analysis*, Cambridge University Press.

Zimmer, M. A., M. Prasad, G. Mavko, and A. Nur (2007), Seismic velocities of unconsolidated sands: Part 1 — Pressure trends from 0.1 to 20 MPa, *GEOPHYSICS*, *72*(1), E1–E13, doi:10.1190/1.2399459.

Zoeppritz, K. (1919), Über Reflexion und Durchgang seismischer Wellen durch Unstetigkeitsflächen, *Nachrichten von der Gesellschaft der Wissenschaften zu Göttingen, Mathematisch-Physikalische Klasse*, *1919*, 66–84.